Rev.Adv.Mater.Sci. 20(2009) 85-91

CALCULATIONS AND MEASUREMENTS OF THE MAGNETIC FIELD OF PATTERNED PERMANENT MAGNETIC FILMS FOR LAB-ON-CHIP APPLICATIONS

Sergey Chigirinsky[1], Mikhail Kustov[1], Nora Dempsey[2], Cheikh Ndao[2] and Rostislav Grechishkin[1]

[1] Laboratory of Magnetoelectronics, Tver State University, 170043 Tver, Russia
[2] Institut Néel, CNRS-UJF, 38042 Grenoble, France

Received: February 03, 2008

Abstract. The growing research in the applications of magnetically patterned thin film permanent magnets (PM) for lab-on-chip micromanipulation of various microscopic objects and for micro-electro-mechanical systems (MEMS) increases the demand for characterization of the magnetic space field distribution produced by such PMs. In the present work calculations are made for different patterns and magnetization distributions of Nd-Fe-B anisotropic films deposited onto 100 mm Si substrates using high rate triode sputtering. Space resolved magnetic imaging techniques utilizing magneto-optical indicator films (MOIF) were applied for the visualization of the magnetic field microdistribution with a resolution of the order of 1 micrometer. Both uniaxial and planar MOIF calibrated with the aid of a known external field were used to achieve quantitative measurements. Deviation of the data measured for real samples from the results of calculations performed for the idealized case of a uniform material are revealed. The obtained results are used both for the characterization of the performance of corresponding devices and for the correction of technological parameters of film preparation.

1. INTRODUCTION

High performance RE-TM magnets have many potential applications in lab-on-chip and MEMS devices. The use of micro-machined bulk magnets is limited by a deterioration of the hard magnetic properties due to surface degradation. What is more, it is not favourable to batch processing nor to further system miniaturisation. The use of film deposition techniques is much more promising. In this case the challenge posed is the attainment of sufficiently thick, high performance, films which are structured at the scale required for lab-on-chip and MEMS devices.

Triode sputtering has been used to prepare highly textured thick NdFeB films with excellent extrinsic magnetic properties [1]. Two patterning routes have been used. Topographically patterned films were produced by deposition onto pre-structured Si substrates. Trenches with widths and pitches in the range of 10 to 100 microns were filled. Magnetically patterned films were produced by thermomagnetic writing using a laser to locally heat the film in a magnetic field. In the present work we report on the calculation and experimental characterization of the magnetic field distribution produced by these patterned films.

2. CALCULATIONS

A favourable feature of modern rare-earth type permanent magnets is that due to their very high anisotropy field and coercive force the residual magnetization vector, $\mu_0 \boldsymbol{M}_r$, is strongly fixed to the

Corresponding author: Rostislav Grechishkin, e-mail: rostislav.grechishkin@tversu.ru

© 2009 Advanced Study Center Co. Ltd.

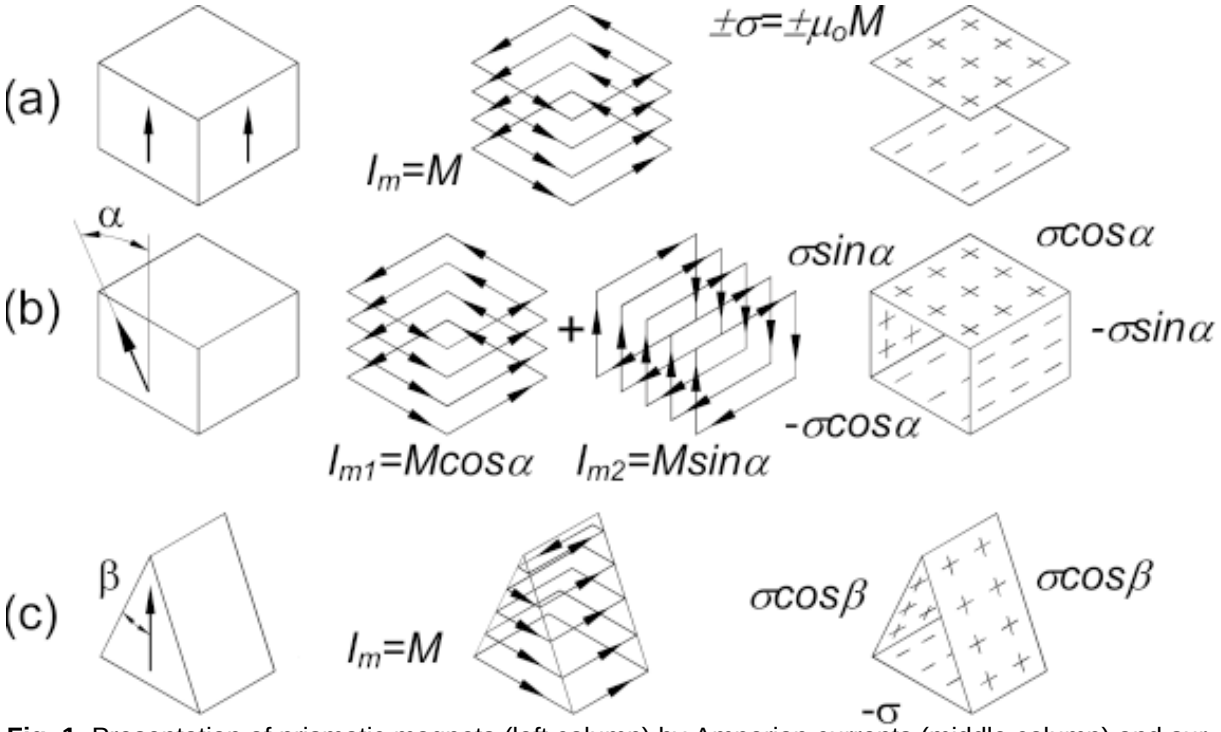

Fig. 1. Presentation of prismatic magnets (left column) by Amperian currents (middle column) and surface magnetic charges (right column).

easy axis of magnetization. Consequently the magnetization remains uniform even in the presence of rather large demagnetizing fields, although the induction may be nonuniform. This rigidity of magnetization radically simplifies the computation of the fields produced by the magnets and justifies the application of superposition principles for systems composed of many elements. In fact, rare-earth magnets are nearly ideal models of uniformly magnetized bodies as represented by surface Amperian currents forming an equivalent solenoid [2]. Thereby the Biot-Savart law, $d\boldsymbol{B} = (\mu_0 I/4\pi)\cdot([d\boldsymbol{l}\times\boldsymbol{R}]/R^3)$, where $\boldsymbol{R}$ is the radius-vector of the point of observation and $[d\boldsymbol{l}\times\boldsymbol{R}] = \boldsymbol{i}\begin{vmatrix} dl_y & dl_z \\ R_y & R_z \end{vmatrix} - \boldsymbol{j}\begin{vmatrix} dl_x & dl_z \\ R_x & R_z \end{vmatrix} + \boldsymbol{k}\begin{vmatrix} dl_x & dl_y \\ R_x & R_y \end{vmatrix}$ is applicable to the calculation of the field of such bodies.

For the particular case of an equivalent solenoid in the form of a rectangular prism $2a'2b'2h$, representing a prismatic magnet magnetized along the z-axis, triple integration of the expressions for dB_x, dB_y and dB_z over the prism sides from $-a$ to a, $-b$ to b and $-h$ to h results in the following simple analytical expressions in terms of elementary functions for magnetic induction values at any point of observation $P(x_0, y_0, z_0)$:

$$
\begin{aligned}
B_x &= -\frac{\mu_0}{4\pi}\frac{I}{2h}\cdot \\
&\left\{\left[\left(\ln\left(\beta+\sqrt{\alpha^2+\beta^2+\gamma^2}\right)\right)_{\alpha_1}^{\alpha_2}\right]_{\beta_1}^{\beta_2}\right\}_{\gamma_1}^{\gamma_2}, \\
B_y &= -\frac{\mu_0}{4\pi}\frac{I}{2h}\cdot \\
&\left\{\left[\left(\ln\left(\alpha+\sqrt{\alpha^2+\beta^2+\gamma^2}\right)\right)_{\alpha_1}^{\alpha_2}\right]_{\beta_1}^{\beta_2}\right\}_{\gamma_1}^{\gamma_2}, \\
B_z &= -\frac{\mu_0}{4\pi}\frac{I}{2h}\cdot \\
&\left\{\left[\left(\tan^{-1}\frac{\gamma+\sqrt{\alpha^2+\beta^2+\gamma^2}}{\alpha\beta}\right)_{\alpha_1}^{\alpha_2}\right]_{\beta_1}^{\beta_2}\right\}_{\gamma_1}^{\gamma_2},
\end{aligned}
\qquad (1)
$$

where α, β and γ are standing for the limits of definite integrals, implying that

$$\left\{\left[f(\alpha,\beta,\gamma)_{\alpha_1}^{\alpha_2}\right]_{\beta_1}^{\beta_2}\right\}_{\gamma_1}^{\gamma_2} = f(\alpha_2\beta_2\gamma_2) - f(\alpha_1\beta_2\gamma_2) - f(\alpha_2\beta_1\gamma_2) + f(\alpha_1\beta_1\gamma_2) - f(\alpha_2\beta_2\gamma_1) + f(\alpha_1\beta_2\gamma_1) + f(\alpha_2\beta_1\gamma_1) - f(\alpha_1\beta_1\gamma_1),$$

where $\alpha_{1,2} = x_0 \pm a$, $\beta_{1,2} = y_0 \pm b$, $z_{1,2} = z_0 \pm h$ (+ and – signs apply to subscripts 1 and 2, respectively). Proceeding to the case of real permanent magnets is carried out by simply replacing the coefficients $\mu_0 I/2h$ in Eqs. (1) – (3) by B_r – residual induction (in Tesla), which is a basic characteristic of a permanent magnet.

Similar formulas may be obtained making use of the formalism of equivalent magnetic charges. An illustration of both representations is given in Fig. 1. In the case of magnetization directions other than along *z*-axis superposition of two or three imaginary bodies with mutually orthogonal magnetization vectors taken in proper proportions is used.

Similar calculations for cylindrical bodies result in the following formulas for the B_x (radial) and B_z (axial) components of the magnetic induction vector at any point of observation $P(x_0, y_0, z_0)$:

$$B_x = \frac{2\mu_0 a}{4\pi}\frac{I}{2h} \times \int_0^{\pi}\left\{\frac{\cos\varphi\, d\varphi}{\left[(z_0 - z)^2 + x_0^2 + a^2 - 2ax_0\cos\varphi\right]^{1/2}}\right\}_{z=-h}^{z=h}, \quad (2)$$

$$B_z = -\frac{2\mu_0 a}{4\pi}\frac{I}{2h}\int_0^{\pi}\frac{(a - x_0\cos\varphi)d\varphi}{x_0^2 + a^2 - 2ax_0\cos\varphi} \times \left\{\frac{(z_0 - z)}{\left[(z_0 - z)^2 + x_0^2 + a^2 - 2ax_0\cos\varphi\right]^{1/2}}\right\}_{z=-h}^{z=h}, \quad (3)$$

Eqs.(2) and (3) could be expressed in terms of complete elliptic integrals of the first and second kind. However, it is simpler to solve these equations by any decent numerical integration routine. Frequently used configurations of axially magnetized rings or cylindrical holes in a matrix are modelled with Eqs. (2) and (3) by a fictitous cylinder with opposite magnetization inserted into the body under consideration.

3. EXPERIMENTAL

Thick films of NdFeB were prepared by high rate triode sputtering as described earlier [1]. Topographically patterned films were achieved by deposition onto prepatterned substrates while magnetically patterned films were prepared by thermomagnetic writing of planar films. Uniaxial and planar magnetooptic indicator films (MOIF) [3,4] were used for qualitative and quantitative analysis of the field distribution at different distances to the patterned film planes.

4. RESULTS AND DISCUSSION

Theoretically calculated B_z/B_r distributions along the *Y* direction at varying distances from the surface of patterned Nd-Fe-B films having different multipole and unidirectional configurations are shown in Fig. 2. It is seen that multipole magnetization along *z*-direction produces the largest amplitudes of the alternating working field (Fig. 2a). However, experimentally it is difficult to magnetize such multipole structures because of the smallness of the pole period, so a good alternative (at the expense of smaller field values) is provided by simple unidirectional magnetization of the patterned structure of Fig. 2b.

The cross-section of a patterned structure prepared as described in [1] is shown in Fig. 3 is, while Fig. 4 illustrates the B_z distribution reconstructed from halftone images obtained with the aid of planar MOIF at a distance of 4 μm from the surface of unidirectionally magnetized sample.

It may be noticed that the distribution shown in Fig. 4c is slightly asymmetrical: top left parts of the $B_z(Y)$ contours are slightly higher and sharper compared to more smooth descending parts at the right sides. Calculations and experiment shows that this effect is due to deviation of the magnetizing field direction from the normal orientation.

Another possibility of producing prescribed magnetic field microdistribution from thin films is provided by thermomagnetic patterning. Experiments were performed with a pulsed Nd-YAG laser heating of NdFeB samples through a mask with holes. During this process the samples were biased by a field of 200 mT. This field is much lower than the room temperature coercive field $\mu_0 H_c \geq 1$ T, so it has no effect on the sample at this temperature, while the $\mu_0 H_c$ falloff during the heating pulse makes the magnetizing or remagnetizing possible.

The calculated and experimental distribution of the magnetic field of thermo-magnetically patterned films with two initial states – that of full thermal demagnetization (cooling from temperatures above Curie point in zero field) or full saturation in nega-

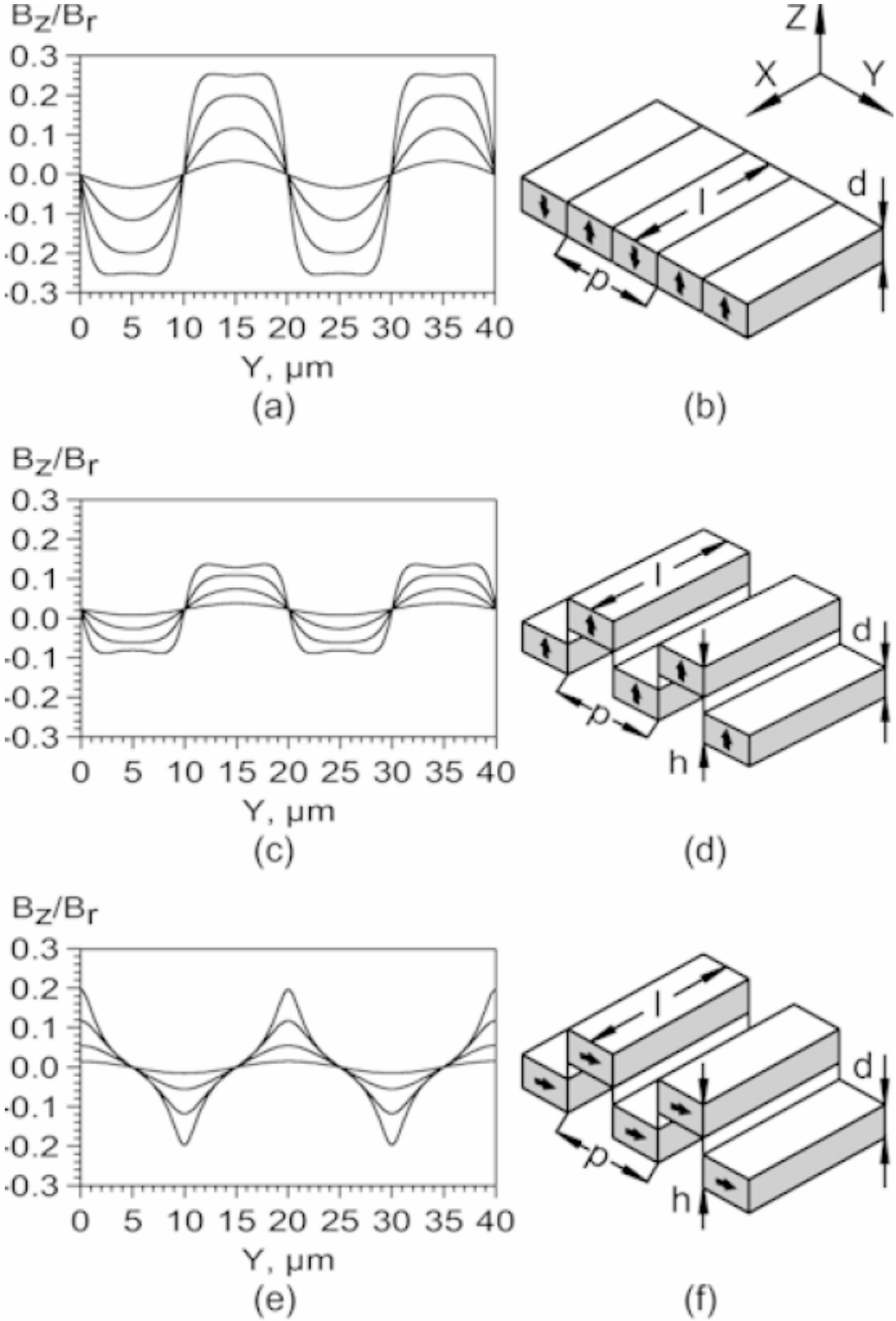

Fig. 2. Theoretically calculated B_z/B_r distribution along the *Y* direction at a distance of 1, 2, 4, and 8 μm from the surface of patterned Nd-Fe-B films of different configurations. [(a), (b)] – multipole magnetization along ±*Z*–direction, [(c), (d)] – unidirectional magnetization of patterned film along +*Z*–direction, [(e), (f)] – unidirectional magnetization the same as [(c), (d)] for magnetization along the +*Y*–direction. *d* – film thickness, *p, h* and *l* – period, height and length of the structure. For the given case *d* = 3.5 μm, *p* = 20 μm, *h* = 10 μm and *l* = 100 μm.

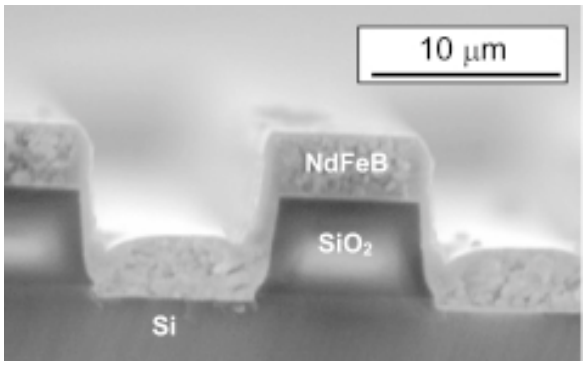

Fig. 3. Cross-section of the NdFeB permanent magnet film deposited on the patterned Si substrate (scanning electron microscopy).

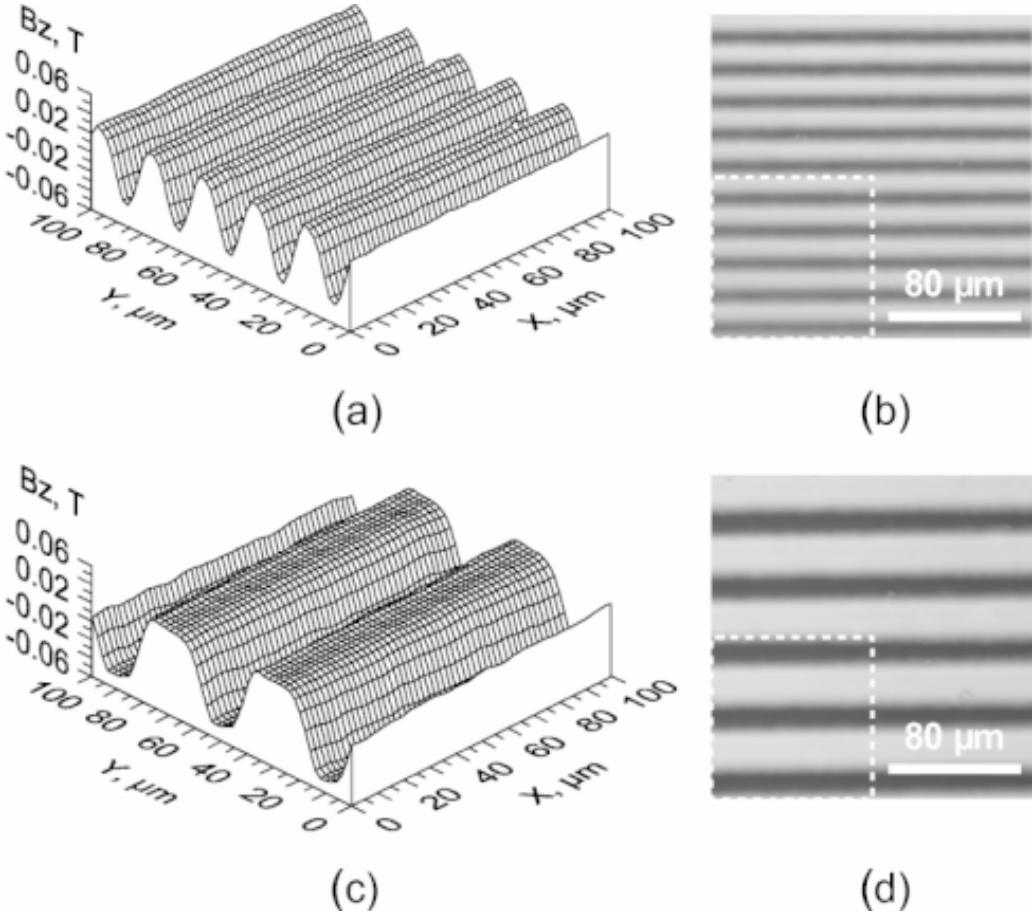

Fig. 4. B_z distribution [(a), (c)] reconstructed from halftone images obtained with the aid of planar MOIF [(b), (d)] at a distance of 4 μm from the surface of unidirectionally magnetized Nd-Fe-B films patterned with a period of 20 and 40 μm period.

tive direction are shown in Fig 5. Thermal magnetizing of square islands exposed to a heating pulse is complete for both cases. For the given geometry patterning of the saturated film produces fields approximately twice as large as compared with the case of initially demagnetized background. Fig. 6 demonstrates a specific effect of 2D periodic film magnetization modulation inside the thermomagnetically written squares. This effect results from the optical diffraction on the perforated mask and serves as an indication of the possible use of interference litography for producing finely divided modulation patterns.

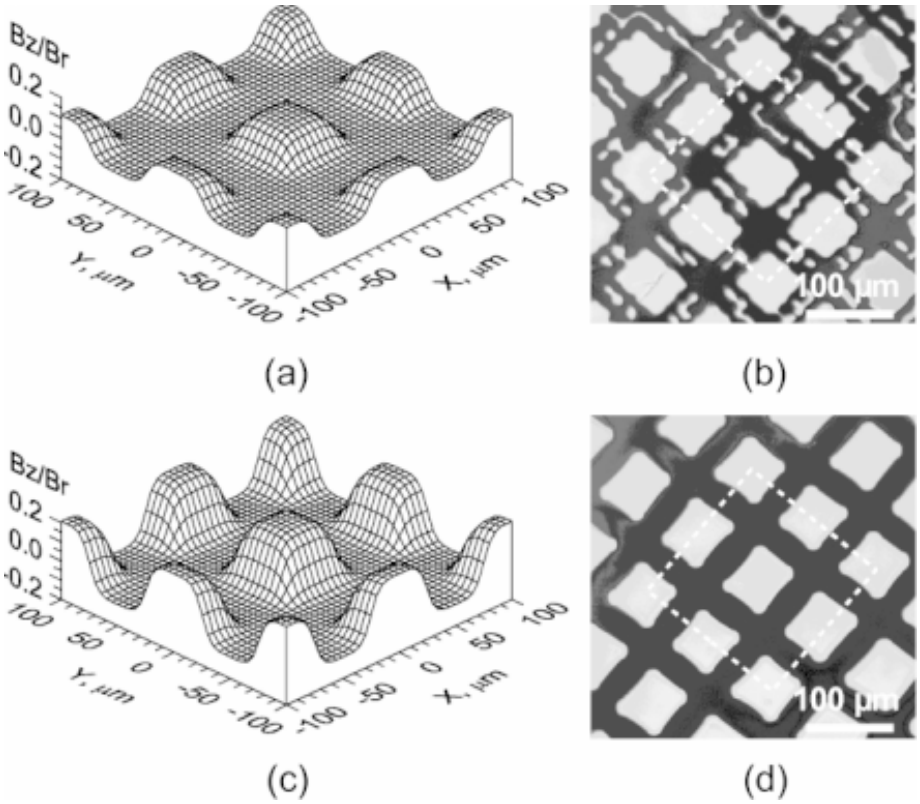

Fig. 5. Theoretically calculated B_z/B_r distribution of the magnetic field at a distance of 4 μm from the surface of Nd-Fe-B film and experimental uniaxial MOIF images of thermomagnetically written 50×50 μm squares. The sample was thermally demagnetized [(a), (b)] or saturated in the negative *z*-direction by a field of 7 T [(c), (d)] before thermomagnetic patterning.

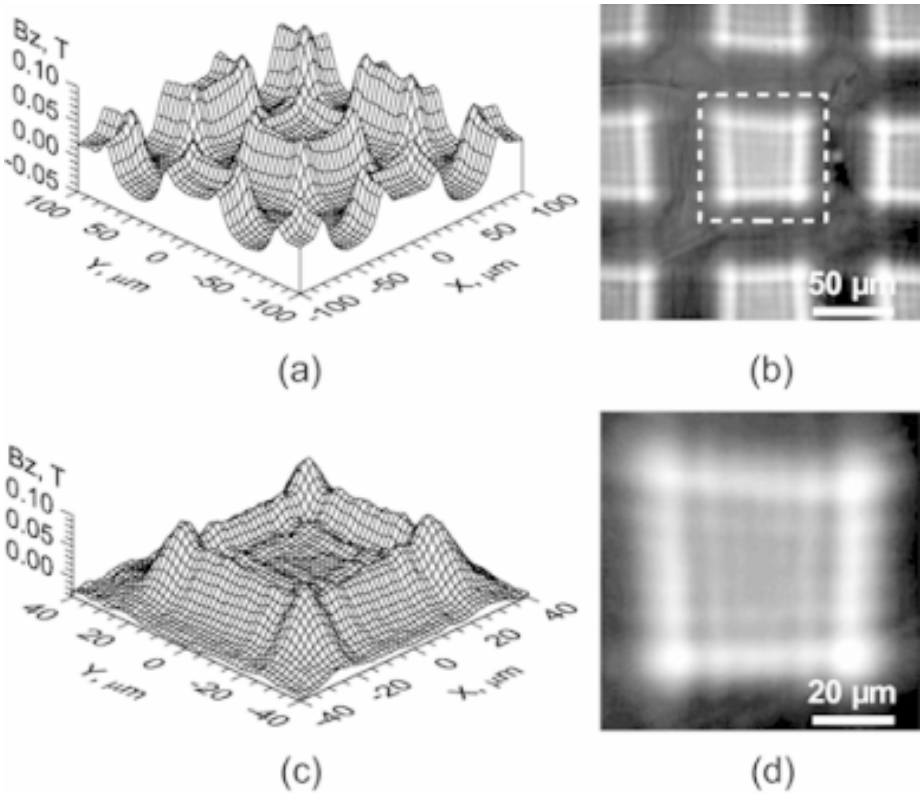

Fig. 6. B_z distribution [(a), (c)] of the magnetic field of Nd-Fe-B film with thermomagnetically written 50×50 μm squares reconstructed from halftone magnetooptic images [(b), (d)] obtained with the aid of planar MOIF. Magnetization modulation with ~12 μm pitch is observed due to Fresnel optical diffraction of the laser beam at the perforated mask .

4. CONCLUSIONS

The magnetron sputtering of patterned NdFeB films in a thickness range of the order of 10 mm on patterned silicon substrates proved to be feasible. A possibility of thermomagnetic patterning of these films with the aid of pulsed laser heating is demonstrated. Comparison of the calculated and experimental data on the magnetic field distribution of patterned films serves to characterize the performance of corresponding devices related to lab-on-chip and MEMS technology [5,6]. Magnetron sputtering of NdFeB films in combination with described specific patterning technology is a promising approach for fabricating complex miniaturized permanent magnet systems.

REFERENCES

[1] N.M. Dempsey, A. Walther, F. May, D. Givord, K. Khlopkov and O. Gutfleisch // *Appl. Phys. Lett.* **90** (2007) 092509.

[2] E.M. Parcell, *Electricity and Magnetism*, *vol. II* (Berkeley Physics Course, McGraw Hill Education, 1986).

[3] R.M. Grechishkin, M.Yu. Goosev, S.E. Ilyashenko and N.S. Neustroev // *J. Magn. Magn. Mater*. **157-158** (1996) 305.

[4] R. Grechishkin, S. Chigirinsky, M. Gusev, O. Cugat and N. Dempsey, In: *Magnetic Nanostructures in Modern Technology*, ed. by B. Azzerboni *et al.* (Springer, 2007), p. 195.

[5] H. Chetouani, C. Jeanday, V. Haquet, H. Rostaing, H. Dieppedale and G. Reyne // *IEEE Trans. Magn*. **42** (2006) 3557.

[6] O. Cugat, G. Reyne, J. Delamare and H. Rostaing // *Sensors and Actuators* **A129** (2006) 265.